

Get a Grip: Reconstructing Hand-Object Stable Grasps in Egocentric Videos

Zhifan Zhu

Dima Damen

School of Computer Science, University of Bristol, UK

<https://zhifanzhu.github.io/getagrip>

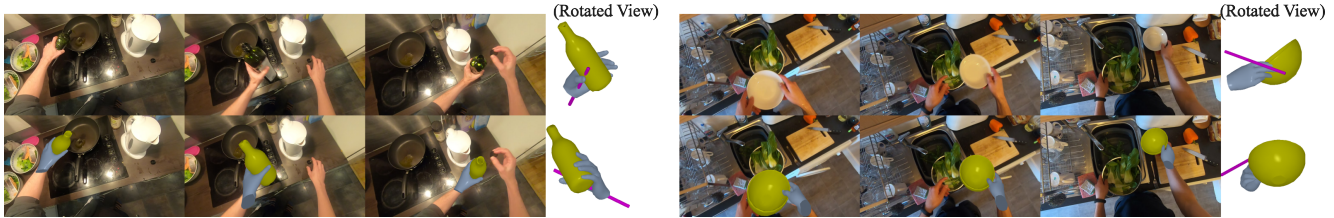


Figure 1. Two stable grasp sequences from EPIC-Grasps for a bottle (left) and bowl (right). We show sample frames (top) and hand-object stable grasp reconstructions (bottom). Right: for each reconstruction, we show the rotated view, along with the latent 1-DoF axis.

Abstract

We address in-the-wild hand-object reconstruction for a known object category in egocentric videos, focusing on temporal periods of stable grasps. We propose the task of Hand-Object Stable Grasp Reconstruction (HO-SGR), the joint reconstruction of frames during which the hand is stably holding the object. We thus can constrain the object motion relative to the hand, effectively regularising the reconstruction and improving performance.

By analysing the 3D ARCTIC dataset, we identify temporal periods where the contact area between the hand and object vertices remain stable. We showcase that objects within stable grasps move within a single degree of freedom (1 DoF). We thus propose a method for jointly optimising all frames within a stable grasp by minimising the object’s rotation to that within a latent 1 DoF.

We then extend this knowledge to in-the-wild egocentric videos by labelling 2.4K clips of stable grasps from the EPIC-KITCHENS dataset. Our proposed EPIC-Grasps dataset includes 390 object instances of 9 categories, featuring stable grasps from videos of daily interactions in 141 environments. Our method achieves significantly better HO-SGR, both qualitatively and by computing the stable grasp area and 2D projection labels of mask overlaps.

1. Introduction

Accurately reconstructing three-dimensional hands along with a grasped or manipulated object is key to unlocking many perception problems, including fine-grained understanding of interactions, but also potential applications including augmented reality, imitation learning and

human-machine interactions.

Prior approaches have laid the foundation for the task, though focusing mostly on 3D input [2, 41, 53], which limits its application to the vast amount of video footage. Approaches with 2D input have relied on 3D ground-truth for supervision [7, 19, 23, 50, 51], again restricting their scope to curated setups where multi-camera sensing and 3D ground truth can be obtained. Early insights [5, 19] demonstrate that evaluation on in-the-wild egocentric footage remains significantly challenging.

In this work, we simplify the task of reconstruction in-the-wild by focusing on temporal periods of stable grasps. Our contribution is composed of four components. **First**, we propose the task of Hand-Object Stable Grasp Reconstruction (HO-SGR) which jointly optimises the reconstructions across all frames within one stable grasp. **Second**, using the ARCTIC dataset [13], we showcase that objects move within one degree of freedom (DoF) once within the hand’s stable grasp. **Third**, we accordingly propose a method that jointly reconstructs the hands and objects by minimising the object’s motion to 1DoF across frames. We demonstrate our method outperforms baselines and alternative assumptions of object movement using 3D ground truth from the stable grasps within the egocentric views of ARCTIC. **Fourth**, we focus on our objective of reconstruction for in-the-wild egocentric videos. We label a sizable dataset of 2.4K stable grasps clips from egocentric videos. Our EPIC-Grasps dataset is the first for hand-object reconstruction collected from unscripted activities, with individuals grasping 390 different objects by both hands. Similar to previous works [5, 6, 15, 17], we restrict our evaluation to known category CAD models. Our dataset comes with pseudo-ground truth in the form of 2D segmentation masks

available from [12], allowing to measure the 3D reconstruction’s projection relative to this 2D groundtruth.

We evaluate our proposed method on EPIC-Grasps, outperforming other baselines using the proxy measure of stable grasps within 2D projections. We demonstrate that joint optimisation within the stable grasp is vital in the egocentric setup as finger joints are often concealed from the camera viewpoint introducing additional ambiguity when reconstructing from a single image.

We demonstrate a sample from our EPIC-Grasps dataset along with reconstructions from our method in Fig 1.

2. Related Works

For comparison of hand object reconstruction datasets, see Sec 5. We review related works in object pose estimation, hand-object reconstruction and grasping.

Object Pose Estimation The task of object pose estimation serves as a foundation for the broader task of hand-object reconstruction. Object pose estimation involves estimating the 6D poses of objects from given CAD models. Labbe and Michaud [27] and Wang et al. [44] proposed instance-level methods for object pose estimation. However, the NOCS method proposed by Wang et al. [45] assumes that no exact CAD models are available and requires an additional size estimation step. To address this limitation, Liu et al. [29] have proposed a method that estimates the 3-DoF sizes of objects, resulting in a 9-DoF pose estimation method.

In this work, we model the object reconstruction as estimating 6D poses with a scalar size, as in [19, 45].

3D Hand-Object-Reconstruction 3D hand object reconstruction methods can be grouped into two categories.

The first category, known-CAD methods [5, 19, 33], assumes that object CAD models are given and fits 3D shapes into 2D observations. To address the limited availability of 3D annotations, several methods [18, 28, 48] have been proposed. Other methods [1, 43, 46, 50] explore hand-object interactions through different modeling approaches. HOMan [19] is a generalisation of single-frame methods that incorporates temporal knowledge through the smoothness of mesh vertices over time and the propagation of object pose initialization using the previous frame’s pose.

The second category, CAD-agnostic methods, aims to estimate the hand and object poses without using explicit CAD models. An early attempt [42] models the object as a 3D bounding box and estimates its 6D pose. More recent methods, such as Diffusion-guided [52], ObMan [20] and implicit shape methods [7, 23, 51], use neural networks to encode the underlying object shape. However, recent methods like Huang et al. [22] require careful scanning of a firmly held object, making them impractical for use in in-the-wild videos.

Our dataset and method belong to the first category, which is a simplified assumption so we focus on the chal-

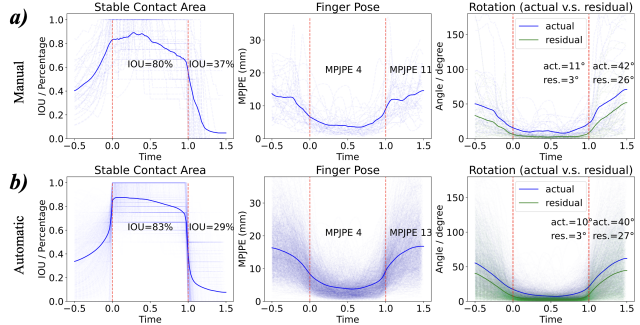


Figure 2. We compare within/outside grasps, analysing object in-contact area (left), finger pose (middle) and relative object rotation w.r.t the hand (right), normalising all stable grasp duration for direct comparison (0 to 1 marked with red dotted lines). We showcase our manual annotations (top) and automatic (bottom). Objects do rotate within the stable grasp (blue) however mostly within 1 DoF (rotation residual in green).

lenges of in-the-wild reconstruction.

3D Human Grasp Synthesis Generating plausible 3D human grasps for objects has been an active area of research.

GraspingField [23] characterises each point in a 3D space as the signed distances to the surfaces of the hand and the object, and learns a generative model to synthesize human grasps. ContactOpt [16] approximates deformable soft tissue in the hand by introducing a differentiable contact model. TOCH [56] learns to refine incorrect 3D hand-object interaction sequences using a correspondence-based prior. Zimeng et al. [55] utilises the physical stability to optimise single-image contact reconstruction.

However, as human grasp synthesis focuses on generating realistic grasps without incorporating input visual information, we do not explore these in this work.

3. What is a “stable grasp”?

The term “stable grasp” has been previously used in a number of prior works [4, 9, 14]. The term intuitively refers to a hand fully supporting the weight of the object, stopping it from slipping or sliding. During interactions, one hand holds an object in a “stable grasp” to either move it from one position to another, or for the second hand to manipulate the object. For example, if one is opening a bottle, then one hand is in a stable grasp while the other hand can be rotating the cap and is thus not in a stable grasp respect to the bottle.

Existing works on grasp type classification implicitly assume the given grasps are stable (or static) [3, 14, 35], without defining what a stable grasp is. Our first contribution is to explore what defines a stable grasp from a video sequence where the hand approaches an object, grasps it, firming the grip into a stable grasp and eventually releases the object. To do so, we leverage the recently introduced ARC-TIC dataset [13]. The data offers a unique opportunity to

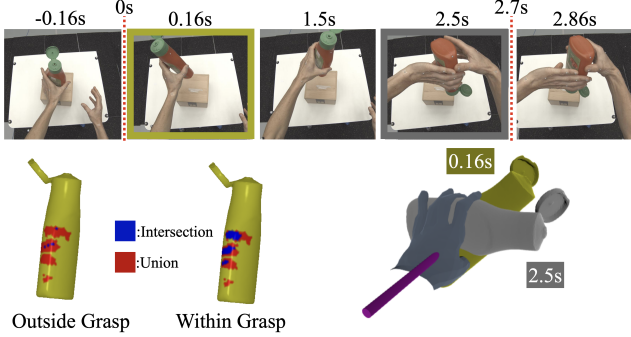


Figure 3. Sample stable grasp sequence from ARCTIC. **Top:** Dotted lines for start-end boundary. **Bottom:** stable contact area and object rotation along 1 DoF (purple).

study hand-object reconstruction as it includes 3D ground truth thanks to being captured in a MoCap system with 54 cameras and markers on both the hand and the objects.

For our exploration, we first analyse the footage and manually annotate 40 temporal extents of what we deem are stable grasps by visual inspection. Figure 2a shows that the stable grasp region corresponds to a consistent in-contact area during the temporal extent of the stable grasp—the same set of object vertices remain in contact with the hand during the grasp but change rapidly outside the grasp. We also demonstrate that both the finger tip poses and the object relative orientations do change during the stable grasps (average MPJPE [13] 4.6mm vs average rotation angle 11.4° for objects). However, these angles are significantly higher outside the stable grasp region (average MPJPE 11.8mm for fingers vs average rotation 42.6° for objects).

Amongst the three metrics, we focus on the stable contact area as it gives the biggest change within/outside grasp. We thus define stable grasp as the temporal segment during which the object in-contact area has high intra-frame IOU

$$[l^*, r^*] = \operatorname{argmax}_{l,r} \{r - l : \text{IOU}(S_i, S_j) > 0.5 \ \forall l \leq i < j \leq r\} \quad (1)$$

where S_i is the object vertices that are in-contact with the hand in frame i . That is the surface in-contact area should remain within an IOU of 0.5 to any other frames during the stable grasp. We use this definition to automatically find all stable grasp temporal boundaries in the ARCTIC dataset.

We accordingly locate 1303 stable grasp clips which we denote these as ARCTIC-Grasps dataset. In Fig 2b we compare this automatic set on the same metrics, showcasing consistent results. On average, 90% of frames have at least 74% IOU between any two frames in the stable grasp.

Object rotation within a stable grasp While object rotations within the stable grasp are consistently low (Fig 2 right), hands are so versatile that objects indeed do rotate, see Fig 3 for example. We observe that these rotations can be successfully approximated by rotations along a single degree-of-freedom (1 DoF). In Fig 2, we show the average

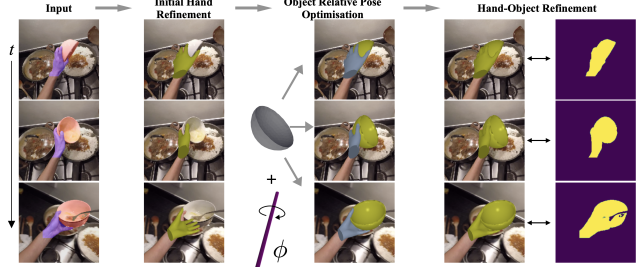


Figure 4. Pipeline overview. We show 3 frames within a stable grasp. The yellow mesh color indicates 3D shapes that are being optimised; the blue mesh color indicates the underlying meshes are frozen. During the object relative pose optimisation stage, the object relative pose is optimised with 1-DoF constraint. During the hand-object refinement stage, the hand mesh and the object mesh are combined, and the ground-truth masks are merged.

rotation versus the rotation off a 1-DoF, calculated as the residual angle off this axis. This residual error is marginal within the stable grasp. In Sec 4.2 we elaborate on how we utilise this knowledge to optimise for hand object reconstructions within the stable grasp boundaries.

From 3D Datasets to Egocentric Videos. As noted in Sec 2 and our introduction, our objective is to perform HO-SGR in-the-wild without any 3D ground truth to assess the reconstruction. The absence of 3D ground truth has been an obstacle for evaluating performance in-the-wild, limiting it to qualitative results solely [19, 52]. By focusing on stable grasps, we offer a way forward to evaluation without 3D ground truth. We use the stable contact area as a measure of assessing successful reconstructions over the duration of the stable grasp. We then use the 1 DoF knowledge in HO-SGR, by minimising the rotation of the object off a latent axis of rotation, within which the object may still rotate. We explain our method next.

4. Method

4.1. Problem Statement and Notations

Given a sequence of images of hand-object interactions, annotated with hand-side, known object category, start-end times of stable grasp and 2D segmentation of the hand and object, we aim to reconstruct consistent grasping, in every sampled frame n of the sequence of length N , by producing a per-frame pair of 3D meshes of the hand and the object w.r.t the camera. We refer to this task as Hand-Object Stable Grasp Reconstruction (HO-SGR).

To represent the **hand mesh**, we use the MANO [36] model, which takes as input a finger articulation vector $\theta \in \mathbb{R}^{45}$ and an identity-specific vector $\beta \in \mathbb{R}^{10}$, and outputs the hand mesh with vertices $V_h \in \mathbb{R}^{778 \times 3}$ in the *hand coordinate system*. We use FrankMocap [37] to obtain MANO finger articulations θ^n from all the frames and we assume the mean hand shape, i.e. $\beta^n = 0$. We thus

have per-frame hand vertices $V_h^n = \text{MANO}(\theta^n, \beta^n)$. The hand-to-camera ($h2c$) pose $T_{h2c}^n \in SE(3)$ [32], which is defined as the hand wrist orientation and position, are produced by FrankMocap by default and are used to transform V_h^n to $V_{h:c}^n$ in the *camera coordinate system* for each frame.

For the **object mesh**, we use $V_o \in \mathbb{R}^{|V_o| \times 3}$ to denote the known object vertices in the *object coordinate system*. We estimate the object-to-hand ($o2h$) poses $T_{o2h}^n \in SE(3)$ and the scale $s \in R$, which transform object vertices to $V_{o:h}^n$ in the *hand coordinate system* for each frame. We then use the hand-to-camera ($h2c$) pose T_{h2c}^n to transform $V_{o:h}^n$ to $V_{o:c}^n$ in the *camera coordinate system* for each frame.

$$V_{o:c}^n = T_{h2c}^n(T_{o2h}^n(s * V_o)) \quad (2)$$

4.2. Reconstructing Objects in a Stable Grasp

The stable grasp segments are defined based on the in-contact surface area, yet it is non-trivial to directly incorporate the Stable Contact Area constraint into optimisation, as the contact area is not known in advance.

Instead, as shown in Sec 3, we constrain the reconstruction so the in-hand object motion is minimised to a single degree-of-freedom, i.e. the object rotates along a fixed latent axis. We represent the 6D object-to-hand transform as a composition of transformation functions

$$T_{o2h}^n = P_{o2h} \circ P_{o2\phi}^{-1} \circ R_\phi^n \circ P_{o2\phi} \quad (3)$$

i.e. a per-frame rotation R_ϕ^n is first applied to the object along the latent axis, defined by $P_{o2\phi}$, then the common object-to-hand transform P_{o2h} is applied. Furthermore, this does not restrict the ability of the hand to move relative to the camera or the wrist to move freely around the joint.

By back-propagating the error through $V_{o:h}^n$, the common parameters across all frames (P_{o2h} , $P_{o2\phi}$, s) as well as the individual frame parameters $\{R_\phi^n\}$ will be optimised jointly.

4.3. Initial Hand Mesh Refinement

Before optimising the object pose, we perform two steps of refinements for the FrankMocap hand output: temporal smoothness and 2D hand mask. We describe these next.

We define a general temporal smoothness function:

$$F_s(\{\mathbf{x}^n\}) = \sum_{n=2}^{N-1} \left| \mathbf{x}^n - \frac{\mathbf{x}^{n-1} + \mathbf{x}^{n+1}}{2} \right|_2^2 \quad (4)$$

We first optimise the finger articulation vector θ^n with the above temporal smoothness objective:

$$E(\{\theta^n\}) = F_s(\{\theta^n\}) \quad (5)$$

Then, we use the projected 2D *hand mask* to optimise the hand pose at every frame. We optimise the hand-to-camera

pose $T_{h2c}^n = [R_h^n | t_h^n]$ for the hand mask pixel difference with ground-truth as well as temporal smoothness of poses:

$$E(\{R_h^n\}, \{t_h^n\}) = F_s(\{R_h^n\}) + F_s(\{t_h^n\}) + \sum_{n=1}^N E_{mask}^n \quad (6)$$

$$E_{mask}^n = |\mathcal{C}_h^n \otimes (\mathcal{M}_h^n - \Pi(V_{h:c}^n))|_2^2 \quad (7)$$

where $\Pi(\cdot)$ is the differentiable projection function [24, 34] and \mathcal{M}_h^n is the hand mask. \mathcal{C}_h^n is the occlusion-aware mask as in [19, 54] which only computes the error within regions of the hand that are not occluded by the grasped object \mathcal{C}_h^n , set to 1 for the hand and background, and 0 for the object.

4.4. Optimising Object Relative Pose

After refining the hand wrist pose T_{h2c}^n and finger articulation θ^n in Sec 4.3, we keep these fixed, and optimise the object relative pose parameters (P_{o2h} , $P_{o2\phi}$, $\{R_\phi^n\}$) and scale s by minimising the following objective function:

$$E(P_{o2h}, P_{o2\phi}, \{R_\phi^n\}, s; \{\theta^n\}, \{T_{h2c}^n\}) = \sum_{n=1}^N \lambda_1 E_{mask}^n + \lambda_2 E_{ins}^n + \lambda_3 E_{clo}^n \quad (8)$$

The term E_{mask} focuses on estimating a reconstruction that best matches the 2D projections of the object masks throughout the sequence. We measure the error via sum of pixel differences:

$$E_{mask}^n = |\mathcal{C}_o^n \otimes (\mathcal{M}_o^n - \Pi(V_{o:c}^n))|_2^2 \quad (9)$$

where \mathcal{M}_o^n is the object mask and $\Pi(\cdot)$ is the differentiable projection function. Similar to our optimisation for hand vertices using the masks, we wish not to penalise parts of the object occluded by the hand. Accordingly, we define the mask \mathcal{C}_o^n such that \mathcal{C}_o^n is 1 for the object and the background, and 0 for the hand.

Similar to [5, 19, 50], we use the physical heuristics E_{ins} , which pushes the object out of the penetrating region against the hand and a balancing loss E_{clo} which pulls the object to touch these contact regions. Please refer to the appendix for more details of the physical heuristics.

The latent axis $P_{o2\phi}$ is initialised at the origin in the object coordinate system and initially points in the $+z$ direction; the R_ϕ^n are initialised to 0. The initialisation of P_{o2h} is described in the implementation details.

4.5. Hand-Object Pose Refinement

In Sec 4.3 the initial hand mesh was refined without the knowledge of the in-hand object. After the optimisation of T_{o2h}^n , we keep the object relative poses fixed and perform two steps of refinement in an object-aware manner.

Refining hand-object as a single mesh. We glue the per-frame pair of meshes of the hand and the object into a single mesh, i.e. $V_{h:o:h}$ as a concatenation of $V_{h:h}$ and $V_{o:h}$.

Dataset	Year	Characteristics			Stats					Labels	
		In-the-wild	Funct. Intent	Ego	#Env	#Sub	#Cat	#Inst	#Seq	Pose GT	Stable Grasp
FPHA [15]	2018	✗	✓	✓	3	6	4	4	1,175	3D	✗
HO3D [17]	2020	✗	✗	✗	1	10	10	10	65	3D	✓(part)
ContactPose [2]	2020	✗	✓	✗	1	50	25	25	2,306	3D	✓
GRAB [41]	2020	✗	✓	✗	1	10	51	51	1,334	3D	✗
H2O [26]	2021	✗	✓	✓	3	4	8	8	24	3D	✗
DexYCB [6]	2021	✗	✗	✗	1	10	20	20	1,000	3D	✗
HOI4D [30]	2022	✗	✓	✓	610	9	20	800	5,000	3D	✗
Assembly101 [38]	2022	✗	✓	✗	1	53	15	15	4,321	3D Hand*	✗
OakInk [49]	2022	✗	✓	✗	1	12	32	100	1,356	3D	✗
ARCTIC [13]	2023	✗	✓	✓	1	9 [†]	11	11	339	3D	✗
ARCTIC-Grasps (ours)	2023	✗	✓	✓	1	9	11	11	1,303	3D	✓
Core50 [31]	2017	✓	✗	✗	11	-	10	50	550	2D Mask	✗
MOW [5, 33]	2021	✓	✓	✗	500	500	121	500	500	✗	✗
EPIC-Grasps (ours)	2023	✓	✓	✓	141	31	9	~390	2,431	2D Mask	✓

Table 1. Dataset Comparison: *: cannot be used for hand-object reconstruction as object poses or segments are not provided. †: subjects in the released train/val set. Two subjects are in the held out test set.

This step refines the hand pose $T_{h2c}^n = [R_h^n | t_h^n]$ so that the combined hand-object mesh aligns better with the combined hand-object mask (Fig 4 right-most column). We then optimise the sum of pixel differences and the smoothness of the object in the camera coordinate system $V_{o:c}^n$:

$$E(\{R_h^n\}, \{t_h^n\}) = F_s(\{V_{o:c}^n\}) + \sum_{n=1}^N E_{mask}^n \quad (10)$$

$$E_{mask}^n = |C_{ho}^n \otimes (\mathcal{M}_{ho}^n - \Pi(V_{ho:c}^n))|_2^2 \quad (11)$$

where C_{ho}^n is 1 for the hand-object and the background, and 0 for other objects; M_{ho}^n is the combined hand-object mask.

Refining finger articulation. As the object has been introduced to the hand, we refine finger articulations such that the hand and object are in plausible contact, using physical constraints E_{ins} and E_{clo} introduced in Sec 4.4:

$$E(\{\theta^n\}) = F_s(\{\theta^n\}) + \sum_{n=1}^N E_{ins}^n + E_{clo}^n \quad (12)$$

As summarised in Fig 4, we perform three stages of optimisation. The first stage refines FrankMocap output using ground-truth hand masks. The second optimises the in-hand object pose using known hand poses and ground-truth object masks. The third refines the hand pose and the finger articulation in an object-aware manner.

5. EPIC-Grasps Annotations

With the definition of stable grasp finalised on in-lab videos of the ARCTIC dataset, we now use this to annotate the temporal extents of stable grasps in unscripted egocentric recordings capturing in-the-wild hand-object stable grasps. This offers a dataset distinct from prior works, where frame-level labels [5, 20, 49], 3D supervision [2, 41,

53] or recordings specifically collected to evaluate grasps with no underlying action [6, 17, 26] are typically used. Instead, we aim to find stable grasps from within egocentric videos recorded of daily actions in an unscripted manner.

We next detail our pipeline to annotate EPIC-Grasps:

1. Identifying candidate clips to annotate. The ultimate goal of hand-object reconstruction is to operate for any rigid or dynamic objects, including novel previously unknown objects. However, current approaches for reconstruction of unknown objects are still in their infancy [22, 39, 40, 51, 52]. We thus restrict our first-attempt at reconstruction in-the-wild to objects for which a category CAD model can be acquired. Note that this is distinct from instance CAD models in ARCTIC-Grasps, for example, the general CAD model of a bottle might not exactly match all bottles in daily life.

We exclude very small objects and shortlist 9 object categories frequently used in kitchens: plate, bowl, bottle, cup, mug, can, pan, saucepan, glass¹.

We begin with the frame-level hand-object interaction annotations from VISOR [12], in which we identified clips where the a hand is in contact with one of the categories above. The annotations also inform us which hand is in contact with the object (i.e. left or right). We then use the fine-grained action labels available from EPIC-KITCHENS [10, 11] to locate the initial temporal extent for actions involving any of these categories. This resulted in 5516 in-action candidate segments.

2. Annotating Stable Grasps. Two annotators were asked to label the start-and-end frames following the stable grasp definition in Sec 3. We discard segments when (i) a segment does not contain any stable grasp (ii) both the hand and object are out-of-view during the sequence (iii) the object does not match the category CAD model specified.

¹For the **object mesh**, we made the CAD model in Blender [8] as the common shape of each category.

3. 2D Hand and Object Segmentation Annotations. In total, we labelled 2431 video clips of stable grasps from 141 distinct videos in 31 kitchens [11]. For each clip, we have a start and end time of the stable grasp, as well as 319,661 segmentation masks for the hand and the object during the stable grasp from the dense VISOR annotations [12]. Of these, 1446 contain left hand stable grasps and 985 contain right hand stable grasps. Note that the majority of subjects recording the EPIC-KITCHENS dataset are right-handed—which implies the left hand is more frequently used to steady the object during manipulation. Compared to previous efforts [6, 17, 26, 30, 40], most clips in EPIC-Grasps contains *both hands in view* manipulating the same or different objects.

Table 1 compares our dataset with currently available and regularly used datasets for hand-object reconstruction. In the first section, we show datasets collected with 3D Ground-Truth. These datasets are limited in the environmental setup to allow for multi-camera views or motion capture tracking. This limits the appearance diversity and interactions are not functional. In Table 1 we also report the functional intent of various dataset (i.e. object is used with intent). our dataset is the first to capture in-the-wild egocentric videos with functional intent. Of particular note is the HOI4D [30] where diversity is targeted with a large number of indoor rooms. However, this is a constructed setup, where objects are selected from a given pool. In EPIC-Grasps, subjects are recording in their actual (personal) kitchens and objects.

6. Experiments

The experiment section is structured as follows: in Sec 6.1 and Sec 6.2 we describe the implementation details of our method and the quantitative metrics respectively. Sec 6.3 and Sec 6.4 report results of our method and baselines on ARCTIC-Grasps and EPIC-Grasps, respectively. Finally Sec 6.5 conducts ablation studies on our method.

6.1. Implementation Details

Finding stable grasps on ARCTIC. We measure the object in-contact area using set of vertices. As individual vertices are sensitive to noise, we partition vertices into fragments using the farthest-point-sampling method, and measure the area using unions of fragments. We set the number of fragments to 0.01 of the number of vertices. As our pipeline assumes rigid object, we exclude segments where the hand is changing the object’s articulation.

Optimisation Pipeline. We follow the convention in HOMan [19] which sparsely and linearly samples 30 frames from the sequence for optimisation and evaluation. We use 50 initialisations of object rotation and 1 global translation

for each object². The optimisation process takes 1.5 minutes on a 2080Ti for one 30-frame sequence on average.

Balancing Error Functions. The error E_{mask} is defined in pixels while E_{ins} and E_{clo} are defined in 3D space (mm), they are related by the camera’s focal length f , thus we introduce a focal scaling factor for E_{ins} and E_{clo} : $\lambda_f = f * render_size$. We use $render_size = 256$ and set $\lambda_1 = 1$, $\lambda_2 = 1 * \lambda_f$ and $\lambda_3 = 0.1 * \lambda_f$; here the focal length f is estimated by FrankMocap.

Please refer to appendix for further implementation details.

6.2. Baselines and Quantitative Metrics

We use 4 baselines to compare to:

- **HOMan [19]**—a common baseline in other works [33, 52] that progressively optimises the object.
- **Single Frame** Single-frame optimisation without utilising the knowledge of stable grasps.
- **Static** A version of our method where objects are not allowed any motion when within the stable grasp, minimising the overall rotation and translation of the object.
- **Dynamic** A variation of our method where objects are allowed to move freely within 6-DoF.

We propose quantitative metrics to measure the correctness of the predicted object poses as well as correctness of the stable grasp. We utilise our stable grasp annotations so as to correctly assess reconstruction with/without 3D ground truth. Specifically, given the knowledge that stable grasps maintain a consistent contact area between the hand and the object throughout the sequence, we measure this contact area over time. However, a reconstruction can maintain a stable contact area but be completely erroneous. We thus propose to combine a measure of correctness of reconstruction with the stability of the contact area to produce a robust metric. We explain this next.

Average Distance (ADD %). Following [21, 25, 47], we measure the distance of corresponding vertices between GT and predicted object vertices in the hand coordinate, and average this distance over vertices and frames. ADD is 1 for a sequence if the average distance is less than 10% of the object’s diameter, and 0 otherwise.

Average Stable Contact Area at ADD Success (SCA-ADD %). When a pose is considered correct for a sequence, i.e. ADD is 1, we measure the Stable Contact Area across the sequence, defined as the average IOU of surface in contact area between each pair of frames 3. SCA-ADD is set to 0 when ADD is 0. We average over all examples.

Intersection-over-Union (IOU %). We use IOU as a proxy of pose accuracy when 3D GT is not available. We measure the Intersection-over-Union between the ground-truth mask

²We use prior knowledge of grasps from ground-truth of ARCTIC to find these initialisations

	Single Frame				HOMan [19]				Static				Dynamic				1-DoF			
	IOU	SCA-IOU	ADD	SCA-ADD	IOU	SCA-IOU	ADD	SCA-ADD	IOU	SCA-IOU	ADD	SCA-ADD	IOU	SCA-IOU	ADD	SCA-ADD	IOU	SCA-IOU	ADD	SCA-ADD
box	93.2	17.5	9.4	3.1	83.5	30.9	33.3	16.9	90.9	67.3	37.7	28.7	95.2	41.7	57.2	25.4	94.2	56.7	39.1	23.6
capsulemachine	79.3	17.8	8.4	3.3	84.0	34.4	42.1	24.5	79.8	34.9	48.4	34.1	88.8	41.6	53.7	29.2	86.1	51.4	62.1	41.2
espressomachine	82.8	19.1	22.8	8.3	84.2	36.9	44.6	28.8	82.6	49.2	48.5	36.2	89.6	43.1	66.3	34.5	87.4	54.9	54.5	35.6
ketchup	81.3	29.3	30.2	16.4	72.0	18.0	15.1	9.3	75.3	32.7	51.9	37.8	89.4	56.0	62.3	40.2	84.0	55.4	64.2	45.0
laptop	87.8	24.9	16.7	7.0	82.1	35.3	43.8	28.0	86.0	62.0	45.1	37.1	93.3	50.2	63.2	34.6	91.4	68.0	54.9	40.8
microwave	85.7	17.1	29.5	8.0	87.0	36.1	56.2	27.3	85.4	51.5	50.9	35.3	90.3	35.2	53.6	23.0	89.0	52.5	55.4	34.8
mixer	79.4	12.1	14.8	4.9	85.3	34.3	45.1	26.7	79.3	37.9	48.4	32.2	89.1	38.4	59.0	29.0	87.0	52.0	62.3	39.6
notebook	87.2	25.0	6.6	2.8	85.7	38.7	33.8	20.8	84.5	57.8	43.0	33.2	93.5	52.8	63.6	35.0	90.9	65.5	55.6	38.7
phone	82.9	25.7	15.1	6.8	80.9	39.5	28.1	19.9	77.8	36.7	39.7	29.2	91.1	58.8	37.7	23.5	88.1	61.9	54.1	37.6
scissors	48.5	0.0	14.0	9.3	40.9	5.2	7.0	5.2	48.2	0.0	47.4	36.3	73.9	18.2	56.1	38.9	62.4	2.7	68.4	51.8
waffleiron	85.7	13.1	3.1	0.9	86.5	36.3	45.0	26.2	84.7	48.3	59.5	39.2	92.7	44.3	81.7	38.1	91.2	55.9	69.5	43.7
All	83.3	19.5	15.0	6.0	81.4	33.1	37.1	22.0	81.4	46.6	46.9	34.2	90.8	45.5	59.6	31.5	88.1	55.7	57.3	38.5

Table 2. Results on ARCTIC-Grasps. Green shows the best performing method per metric and yellow shows second best.

and the rendered mask for the object in camera view. We report average IOU across all frames. Due to occlusion with other components in the scene, only the non-occluded area of the rendered projection is used.

Average Stable Contact Area at high IOU (SCA-IOU %). Using IOU as proxy for correct reconstructions, we analogously report SCA when IOU is more than certain thresholds. We use 80% as threshold on ARCTIC-Grasps and report both 80% and 60% on EPIC-Grasps. SCA-IOU is set to 0 when IOU is below the threshold. We report average SCA-IOU.

The first 2 metrics, ADD and SCA-ADD, are evaluated when 3D ground truths are available—e.g. ARCTIC-Grasps dataset; and the other two are the corresponding 2D proxy, which we use for EPIC-Grasps.

6.3. Results on ARCTIC-Grasps

Table 2 compares results on ARCTIC-Grasps dataset using all the metrics. We focus solely on the object stable grasp optimisation in the ARCTIC-Grasps dataset, thus using ground-truth hand mesh and camera parameters. We also use a known scale for the object. We thus do not use the hand refinement stages to report these results.

While Dynamic and 1-DoF both have significantly higher ADD results, 1-DoF maintains the best SCA when grasps are successfully reconstructed (high SCA-ADD). While Static has considerably high SCA, its IOU and ADD are significantly lower than 1-DoF in every category. HOMan only performs best on the “microwave” object sequences. Single Frame performs worst in every case.

6.4. Results on EPIC-Grasps

Table 3 compares results on EPIC-Grasps dataset using proxy metrics IOU and SCA-IOU. We also report SCA-IOU at IOU threshold 0.6 since the overall IOU for are lower. We evaluate two best variations based on 3D performance on ARCTIC-Grasps: Dynamic and 1-DoF. 1-DoF achieves the best SCA-IOU metric for both thresholds for every object category and overall.

Figure 5 shows reconstruction results of our 1-DoF approach on the EPIC-Grasps dataset. We showcase three examples per category. From the images, the challenge in EPIC-Grasps dataset is evident with the hand and object occupying a small proportion of the image. In most examples,

	HOMan [19]			Dynamic			1-DoF		
	IOU	SCA@0.8	SCA@0.6	IOU	SCA@0.8	SCA@0.6	IOU	SCA@0.8	SCA@0.6
bottle	56.7	3.4	5.8	64.8	7.0	20.4	62.7	10.2	33.1
bowl	54.4	1.1	1.6	58.5	7.6	12.4	57.2	12.2	22.2
can	48.3	3.4	5.1	52.4	10.1	15.4	52.4	12.7	24.6
cup	56.9	5.5	7.8	61.4	6.0	24.2	60.3	10.1	36.8
glass	55.4	3.0	4.2	60.2	8.2	21.7	57.5	10.2	29.7
mug	59.4	3.9	6.6	59.0	5.0	18.0	60.1	6.7	28.7
pan	48.4	0.5	1.9	47.0	2.5	6.9	47.5	4.4	13.5
plate	61.1	1.0	1.6	67.1	12.9	19.3	66.6	18.7	30.3
saucepan	51.1	0.4	2.4	57.2	3.4	11.5	55.9	9.0	19.7
All	54.9	1.9	3.3	58.6	7.2	15.5	57.8	10.8	25.2

Table 3. Results on EPIC-Grasps. Green for best method and yellow shows second best.

	Static		Dynamic		1-DoF	
	ADD	SCA-ADD	ADD	SCA-ADD	ADD	SCA-ADD
Within	45.0	31.4	55.0	26.7	54.0	33.3
Outside	11.0	6.9	46.0	15.1	27.0	12.9

Table 4. Within/Outside grasps on ARCTIC-Grasps Sequences.

the palm and fingers are concealed. Importantly, all grasps are functional – e.g. picking a cup from the drainer.

Figure 6 shows comparative results. Despite acceptable overlay, HOMan does not maintain the stable grasp and the object is in fact sliding in the hand over time. The Dynamic baseline has significantly lower SCA with the contact area drifting over time. Our proposed 1-DoF method is able to reconstruct the stable grasp as it benefits from the constrained relative pose assumption.

While results in-the-wild are very promising, our pipeline relies on FrankMocap as a first stage. Despite the robustness incorporated by the multiple-view joint optimisation, our method fails when the majority of hand poses are incorrect (see Fig 7).

6.5. Ablation Studies

What happens outside the stable grasp boundary? In Table 4 we show results when we remove the knowledge of the grasp start-end time. We run this ablation on a random subset of ARCTIC-Grasps dataset of 100 sequences, for tractable processing. We extend the start-end time of the boundary by 0.5s on both sides.

Clearly, all methods show a drop in performance, as some of these frames might not even have the hand in grasp of the object. Dynamic has the least drop as it does not have a constraint to optimise.

Ablation on Refinement Table 5 presents the impact of performing two refinements on our method. The final re-

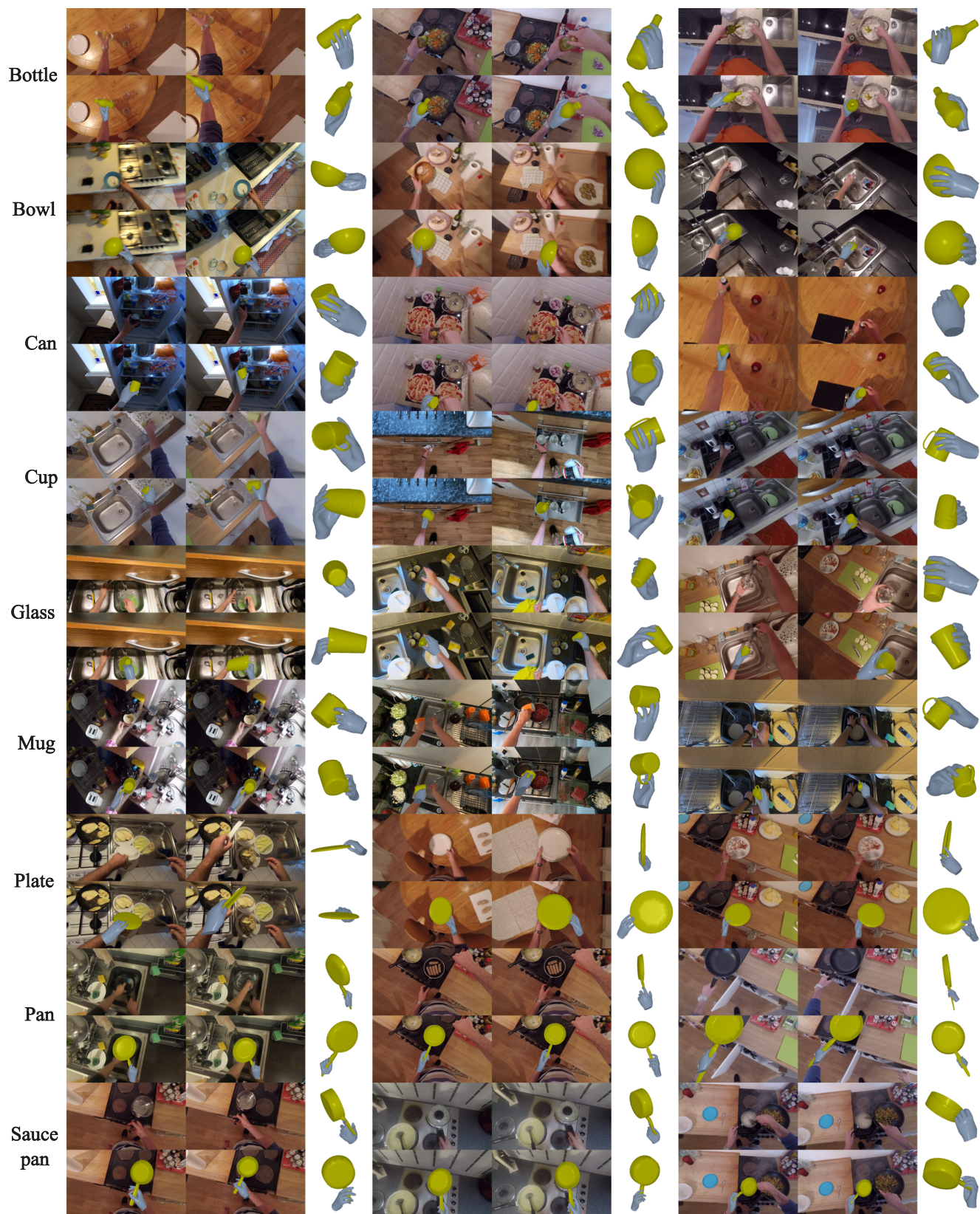


Figure 5. Qualitative Results on EPIC-Grasps (3 examples per category); input frames (top), projected reconstruction results (bottom) and reconstruction in rotated views (right).

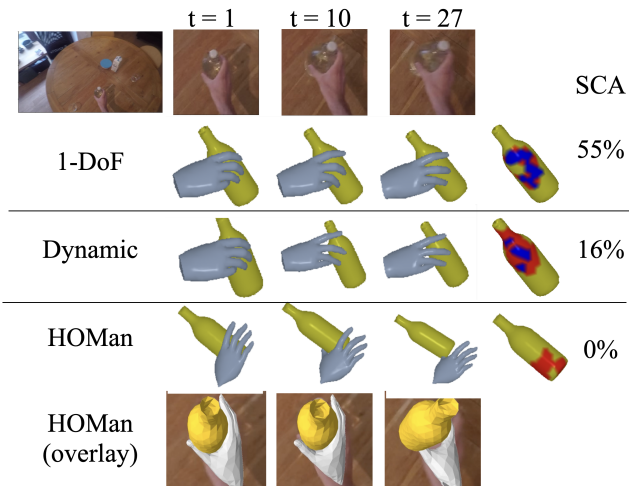


Figure 6. Qualitative comparison between 1-DoF, Dynamic and HOMan [19]. We show input frames (top), grasp reconstruction results and the corresponding SCA.

Init Refine	HO Refine	IOU	SCA@0.8	SCA@0.6
✗	✗	54.1	6.4	18.9
✗	✓	54.7	9.2	23.4
✓	✓	57.8	10.8	25.2

Table 5. Impact of refinement stages on EPIC-Grasps.



Figure 7. Failure Case in EPIC-GRASPS due to FrankMocap.

finement stage alone leads to a small improvement; when using both refinement stages, this leads to an average increase of 3.6% in IOU and 7.4% in SCA@0.6.

7. Conclusion

In this paper we build a challenging in-the-wild egocentric videos dataset for hand-object reconstruction. The dataset contains 2D masks as pseudo ground-truths and manual temporal labels of stable grasps. By focusing on stable grasps, we can jointly optimise multiple frames given the knowledge of how objects move relative to the hand within grasp. We evaluate the method’s ability to achieve a stable grasp without 3D ground truth by approximating the 2D IOU of object masks along with measuring the stable contact area over time.

By investigation stable grasps, we hope to encourage more methods to quantitatively evaluate methods in-the-

wild. An obvious limitation of our approach is its reliance on the knowledge of the category’s CAD model. Current CAD-agnostic methods struggle in-the-wild – we showcase failures in appendix [51]. However, removing the limitation of CAD model knowledge is a clear future direction.

Acknowledgements. Research is supported by EPSRC UMPIRE (EP/T004991/1). Z. Zhu is supported by UoB-CSC Scholarship.

References

- [1] Ahmed Tawfik Aboukhadra, Jameel Malik, Ahmed Elhayek, Nadia Robertini, and Didier Stricker. Thor-net: End-to-end graformer-based realistic two hands and object reconstruction with self-supervision. In *Proceedings of the IEEE/CVF Winter Conference on Applications of Computer Vision*, pages 1001–1010, 2023. 2
- [2] Samarth Brahmabhatt, Chengcheng Tang, Christopher D Twigg, Charles C Kemp, and James Hays. Contactpose: A dataset of grasps with object contact and hand pose. In *Proceedings of the European Conference on Computer Vision (ECCV)*, pages 361–378, 2020. 1, 5
- [3] Ian M. Bullock, Thomas Feix, and Aaron M. Dollar. The Yale human grasping dataset: Grasp, object, and task data in household and machine shop environments. *International Journal of Robotics Research*, 34(3):251–255, 2015. 2
- [4] Ian M. Bullock, Raymond R. Ma, and Aaron M. Dollar. A hand-centric classification of human and robot dexterous manipulation. *IEEE Transactions on Haptics*, 6(2):129–144, 2013. 2
- [5] Zhe Cao, Ilija Radosavovic, Angjoo Kanazawa, and Jitendra Malik. Reconstructing hand-object interactions in the wild. In *Proceedings of the IEEE/CVF International Conference on Computer Vision*, pages 12417–12426, 2021. 1, 2, 4, 5
- [6] Yu-Wei Chao, Wei Yang, Yu Xiang, Pavlo Molchanov, Ankur Handa, Jonathan Tremblay, Yashraj S Narang, Karl Van Wyk, Umar Iqbal, Stan Birchfield, et al. Dexycb: A benchmark for capturing hand grasping of objects. In *Proceedings of the IEEE/CVF Conference on Computer Vision and Pattern Recognition*, pages 9044–9053, 2021. 1, 5, 6
- [7] Zerui Chen, Yana Hasson, Cordelia Schmid, and Ivan Laptev. Alignsdf: Pose-aligned signed distance fields for hand-object reconstruction. In *Proceedings of the European Conference on Computer Vision (ECCV)*, pages 231–248, 2022. 1, 2
- [8] Blender Online Community. *Blender - a 3D modelling and rendering package*. Blender Foundation, Stichting Blender Foundation, Amsterdam, 2018. 5
- [9] M.R. Cutkosky. On grasp choice, grasp models, and the design of hands for manufacturing tasks. *IEEE Transactions on Robotics and Automation*, 5(3):269–279, 1989. 2
- [10] Dima Damen, Hazel Doughty, Giovanni Maria Farinella, Sanja Fidler, Antonino Furnari, Evangelos Kazakos, Davide Moltisanti, Jonathan Munro, Toby Perrett, Will Price, et al. Scaling egocentric vision: The epic-kitchens dataset. In *Proceedings of the European Conference on Computer Vision (ECCV)*, pages 720–736, 2018. 5

- [11] Dima Damen, Hazel Doughty, Giovanni Maria Farinella, Antonino Furnari, Jian Ma, Evangelos Kazakos, Davide Moltisanti, Jonathan Munro, Toby Perrett, Will Price, and Michael Wray. Rescaling egocentric vision: Collection, pipeline and challenges for epic-kitchens-100. *International Journal of Computer Vision (IJCV)*, 130:33–55, 2022. 5, 6
- [12] Ahmad Darkhalil, Dandan Shan, Bin Zhu, Jian Ma, Amlan Kar, Richard Higgins, Sanja Fidler, David Fouhey, and Dima Damen. Epic-kitchens visor benchmark: Video segmentations and object relations. In *Proceedings of the Neural Information Processing Systems (NeurIPS) Track on Datasets and Benchmarks*, 2022. 2, 5, 6
- [13] Zicong Fan, Omid Taheri, Dimitrios Tzionas, Muhammed Kocabas, Manuel Kaufmann, Michael J. Black, and Otmar Hilliges. ARCTIC: A dataset for dexterous bimanual hand-object manipulation. In *Proceedings IEEE Conference on Computer Vision and Pattern Recognition*, 2023. 1, 2, 3, 5
- [14] Thomas Feix, Javier Romero, Heinz Bodo Schmiemayer, Aaron M. Dollar, and Danica Kragic. The GRASP Taxonomy of Human Grasp Types. *IEEE Transactions on Human-Machine Systems*, 46(1):66–77, 2016. 2
- [15] Guillermo Garcia-Hernando, Shanxin Yuan, Seungryul Baek, and Tae-Kyun Kim. First-person hand action benchmark with RGB-D videos and 3d hand pose annotations. In *Proceedings of the IEEE Conference on Computer Vision and Pattern Recognition*, pages 409–419, 2018. 1, 5
- [16] Patrick Grady, Chengcheng Tang, Christopher D Twigg, Minh Vo, Samarth Brahmabhatt, and Charles C Kemp. Contactopt: Optimizing contact to improve grasps. In *Proceedings of the IEEE/CVF Conference on Computer Vision and Pattern Recognition*, pages 1471–1481, 2021. 2
- [17] Shreyas Hampali, Mahdi Rad, Markus Oberweger, and Vincent Lepetit. Honnotate: A method for 3d annotation of hand and object poses. In *Proceedings of the IEEE/CVF Conference on Computer Vision and Pattern Recognition*, pages 3193–3203, 2020. 1, 5, 6, 12
- [18] Yana Hasson, Bugra Tekin, Federica Bogo, Ivan Laptev, Marc Pollefeys, and Cordelia Schmid. Leveraging photometric consistency over time for sparsely supervised hand-object reconstruction. In *Proceedings of the IEEE/CVF Conference on Computer Vision and Pattern Recognition*, pages 568–577, 2020. 2
- [19] Yana Hasson, Gül Varol, Cordelia Schmid, and Ivan Laptev. Towards unconstrained joint hand-object reconstruction from rgb videos. In *2021 International Conference on 3D Vision (3DV)*, pages 659–668, 2021. 1, 2, 3, 4, 6, 7, 9
- [20] Yana Hasson, Gül Varol, Dimitrios Tzionas, Igor Kalevatykh, Michael J. Black, Ivan Laptev, and Cordelia Schmid. Learning joint reconstruction of hands and manipulated objects. In *Proceedings of the IEEE Conference on Computer Vision and Pattern Recognition*, pages 11807–11816, 2019. 2, 5
- [21] Tomas Hodan, Daniel Barath, and Jiri Matas. Epos: Estimating 6d pose of objects with symmetries. In *Proceedings of the IEEE/CVF conference on computer vision and pattern recognition*, pages 11703–11712, 2020. 6
- [22] Di Huang, Xiaopeng Ji, Xingyi He, Jiaming Sun, Tong He, Qing Shuai, Wanli Ouyang, and Xiaowei Zhou. Reconstructing Hand-Held Objects from Monocular Video. In *Proceedings of SIGGRAPH Asia 2022 Conference Papers*, 2022. 2, 5, 12
- [23] Korrawe Karunratanakul, Jinlong Yang, Yan Zhang, Michael J Black, Krikamol Muandet, and Siyu Tang. Grasping field: Learning implicit representations for human grasps. In *2020 International Conference on 3D Vision (3DV)*, pages 333–344, 2020. 1, 2
- [24] Hiroharu Kato, Yoshitaka Ushiku, and Tatsuya Harada. Neural 3d mesh renderer. In *Proceedings of the IEEE Conference on Computer Vision and Pattern Recognition*, pages 3907–3916, 2018. 4
- [25] Alexander Krull, Eric Brachmann, Frank Michel, Michael Ying Yang, Stefan Gumhold, and Carsten Rother. Learning analysis-by-synthesis for 6d pose estimation in rgb-d images. In *Proceedings of the IEEE international conference on computer vision*, pages 954–962, 2015. 6
- [26] Taemin Kwon, Bugra Tekin, Jan Stühmer, Federica Bogo, and Marc Pollefeys. H2o: Two hands manipulating objects for first person interaction recognition. In *Proceedings of the IEEE/CVF International Conference on Computer Vision*, pages 10138–10148, 2021. 5, 6
- [27] Yann Labbé, Justin Carpentier, Mathieu Aubry, and Josef Sivic. Cosypose: Consistent multi-view multi-object 6d pose estimation. In *Proceedings of the European Conference on Computer Vision (ECCV)*, pages 574–591, 2020. 2
- [28] Shaowei Liu, Hanwen Jiang, Jiarui Xu, Sifei Liu, and Xiaolong Wang. Semi-supervised 3d hand-object poses estimation with interactions in time. In *Proceedings of the IEEE/CVF Conference on Computer Vision and Pattern Recognition*, pages 14687–14697, 2021. 2
- [29] Xingyu Liu, Gu Wang, Yi Li, and Xiangyang Ji. Catre: Iterative point clouds alignment for category-level object pose refinement. In *Proceedings of the European Conference on Computer Vision (ECCV)*, pages 499–516, 2022. 2
- [30] Yunze Liu, Yun Liu, Che Jiang, Kangbo Lyu, Weikang Wan, Hao Shen, Boqiang Liang, Zhoujie Fu, He Wang, and Li Yi. Hoi4d: A 4d egocentric dataset for category-level human-object interaction. In *Proceedings of the IEEE/CVF Conference on Computer Vision and Pattern Recognition*, pages 21013–21022, 2022. 5, 6
- [31] Vincenzo Lomonaco and Davide Maltoni. Core50: a new dataset and benchmark for continuous object recognition. In *Conference on Robot Learning*, pages 17–26, 2017. 5
- [32] Yi Ma, Stefano Soatto, Jana Kosecka, and S. Shankar Sastry. *An Invitation to 3-D Vision: From Images to Geometric Models*. SpringerVerlag, 2003. 4
- [33] Austin Patel, Andrew Wang, Ilija Radosavovic, and Jitendra Malik. Learning to imitate object interactions from internet videos. *arXiv preprint arXiv:2211.13225*, 2022. 2, 5, 6
- [34] Nikhila Ravi, Jeremy Reizenstein, David Novotny, Taylor Gordon, Wan-Yen Lo, Justin Johnson, and Georgia Gkioxari. Accelerating 3d deep learning with pytorch3d. *arXiv preprint arXiv:2007.08501*, 2020. 4
- [35] Grégory Rogez, James Steven Supancic III, and Deva Ramanan. Understanding everyday hands in action from RGB-D images. In *Proceedings of International Conference on Computer Vision, 2015*, pages 3889–3897, 2015. 2

- [36] Javier Romero, Dimitrios Tzionas, and Michael J Black. Embodied Hands: Modeling and Capturing Hands and Bodies Together. *ACM Trans. Graph*, 36:17, 2017. 3
- [37] Yu Rong, Takaaki Shiratori, and Hanbyul Joo. Frankmocap: A monocular 3d whole-body pose estimation system via regression and integration. In *Proceedings of the IEEE/CVF International Conference on Computer Vision Workshop*, pages 1749–1759, 2021. 3
- [38] Fadime Sener, Dibiyadip Chatterjee, Daniel Sheleпов, Kun He, Dipika Singhania, Robert Wang, and Angela Yao. Assembly101: A large-scale multi-view video dataset for understanding procedural activities. In *Proceedings of the IEEE/CVF Conference on Computer Vision and Pattern Recognition*, pages 21096–21106, 2022. 5
- [39] Edgar Sucar, Kentaro Wada, and Andrew Davison. NodeSLAM: Neural Object Descriptors for Multi-View Shape Reconstruction. In *Proceedings of the International Conference on 3D Vision (3DV)*, 2020. 5
- [40] Anilkumar Swamy, Vincent Leroy, Philippe Weinzaepfel, Fabien Baradel, Salma Galaoui, Romain Brégier, Matthieu Armando, Jean-Sebastien Franco, and Grégory Rogez. Showme: Benchmarking object-agnostic hand-object 3d reconstruction. In *Proceedings of the IEEE/CVF International Conference on Computer Vision Workshop*, pages 1935–1944, 2023. 5, 6
- [41] Omid Taheri, Nima Ghorbani, Michael J Black, and Dimitrios Tzionas. Grab: A dataset of whole-body human grasping of objects. In *Proceedings of the European Conference on Computer Vision (ECCV)*, pages 581–600, 2020. 1, 5
- [42] Bugra Tekin, Federica Bogo, and Marc Pollefeys. H+O: unified egocentric recognition of 3d hand-object poses and interactions. In *Proceedings of the IEEE Conference on Computer Vision and Pattern Recognition*, pages 4511–4520, 2019. 2
- [43] Tze Ho Elden Tse, Kwang In Kim, Ales Leonardis, and Hyung Jin Chang. Collaborative learning for hand and object reconstruction with attention-guided graph convolution. In *Proceedings of the IEEE/CVF Conference on Computer Vision and Pattern Recognition*, pages 1664–1674, 2022. 2
- [44] Gu Wang, Fabian Manhardt, Xingyu Liu, Xiangyang Ji, and Federico Tombari. Occlusion-Aware Self-Supervised Monocular 6D Object Pose Estimation. *IEEE Transactions on Pattern Analysis and Machine Intelligence*, 2021. 2
- [45] He Wang, Srinath Sridhar, Jingwei Huang, Julien Valentin, Shuran Song, and Leonidas J. Guibas. Normalized object coordinate space for category-level 6d object pose and size estimation. In *Proceedings of the IEEE Conference on Computer Vision and Pattern Recognition*, pages 2642–2651, 2019. 2
- [46] Rong Wang, Wei Mao, and Hongdong Li. Interacting hand-object pose estimation via dense mutual attention. In *Proceedings of the IEEE/CVF Winter Conference on Applications of Computer Vision*, pages 5735–5745, 2023. 2
- [47] Yu Xiang, Tanner Schmidt, Venkatraman Narayanan, and Dieter Fox. Posecnn: A convolutional neural network for 6d object pose estimation in cluttered scenes. *arXiv preprint arXiv:1711.00199*, 2017. 6
- [48] Lixin Yang, Kailin Li, Xinyu Zhan, Jun Lv, Wenqiang Xu, Jiefeng Li, and Cewu Lu. Artiboost: Boosting articulated 3d hand-object pose estimation via online exploration and synthesis. In *Proceedings of the IEEE/CVF Conference on Computer Vision and Pattern Recognition*, pages 2750–2760, 2022. 2
- [49] Lixin Yang, Kailin Li, Xinyu Zhan, Fei Wu, Anran Xu, Liu Liu, and Cewu Lu. Oakink: A large-scale knowledge repository for understanding hand-object interaction. In *Proceedings of the IEEE/CVF Conference on Computer Vision and Pattern Recognition*, pages 20953–20962, 2022. 5
- [50] Lixin Yang, Xinyu Zhan, Kailin Li, Wenqiang Xu, Jiefeng Li, and Cewu Lu. Cpf: Learning a contact potential field to model the hand-object interaction. In *Proceedings of the IEEE/CVF International Conference on Computer Vision*, pages 11097–11106, 2021. 1, 2, 4
- [51] Yufei Ye, Abhinav Gupta, and Shubham Tulsiani. What’s in your hands? 3d reconstruction of generic objects in hands. In *Proceedings of the IEEE/CVF Conference on Computer Vision and Pattern Recognition*, pages 3895–3905, 2022. 1, 2, 5, 9, 12
- [52] Yufei Ye, Poorvi Hebbar, Abhinav Gupta, and Shubham Tulsiani. Diffusion-guided reconstruction of everyday hand-object interaction clips. In *Proceedings of the IEEE/CVF International Conference on Computer Vision*, pages 19717–19728, 2023. 2, 3, 5, 6
- [53] He Zhang, Yuting Ye, Takaaki Shiratori, and Taku Komura. ManipNet: Neural Manipulation Synthesis with a Hand-Object Spatial Representation. *ACM Transactions on Graphics*, 40(4), 2021. 1, 5
- [54] Jason Y Zhang, Sam Pepose, Hanbyul Joo, Deva Ramanan, Jitendra Malik, and Angjoo Kanazawa. Perceiving 3d human-object spatial arrangements from a single image in the wild. In *Proceedings of the European Conference on Computer Vision (ECCV)*, pages 34–51, 2020. 4
- [55] Zimeng Zhao, Binghui Zuo, Wei Xie, and Yangang Wang. Stability-driven contact reconstruction from monocular color images. In *Proceedings of the IEEE/CVF Conference on Computer Vision and Pattern Recognition*, pages 1643–1653, 2022. 2
- [56] Keyang Zhou, Bharat Lal Bhatnagar, Jan Eric Lenssen, and Gerard Pons-Moll. Toch: Spatio-temporal object-to-hand correspondence for motion refinement. In *Proceedings of the European Conference on Computer Vision (ECCV)*, pages 1–19, 2022. 2

Appendix

This appendix is structured as follows: in Sec. A we presents statistics of EPIC-Grasps annotation. Sec. B showcases failure of current CAD-agnostic approach on EPIC-Grasps dataset. Sec. C provides further implementation details.

A. Statistics of EPIC-Grasps annotation

In Table 6, we present average, standard deviation and maximum clip length for each of our categories as well as total number of video clips per category. Note that grasping some categories (e.g. Pan) can be significantly longer in duration than others (e.g. Mug).

category	length (sec)			#-clips
	avg	std.	max	
Bottle	4.25	4.70	29.40	311
Bowl	3.59	5.53	43.36	421
Can	3.50	4.11	22.76	105
Cup	2.79	3.20	19.72	125
Glass	2.45	3.73	34.72	226
Mug	2.40	3.34	29.74	167
Pan	6.39	9.36	91.28	526
Plate	2.77	4.49	54.60	473
Saucepan	5.73	10.08	76.10	77
All	3.95	6.30	91.28	2431

Table 6. EPIC-Grasps sequences statistics

B. Evaluating CAD-agnostic method Ihoi

In our method, we assume knowledge of the CAD model. We also explored the latest works that attempt hand grasps without such knowledge. In this section, we showcase these models to be unusable for our in-the-wild scenes through three example, qualitatively.

The recent shape reconstruction method proposed in [22] requires careful scan of the underlying in-hand object hence is not suitable for testing in our case. Therefore, we evaluate the state-of-the-art image-based CAD-agnostic method Ihoi [51] on the EPIC-Grasps dataset, using a model trained on HO3D [17] images that contain the similar categories: mug and bottle – i.e. the method is aware of these shapes during training. Figure 8 shows Ihoi is unable to generate plausible object meshes.

C. Further Implementation Details

Physical Heuristics In Eq (8) of the main paper we note our usage of physical attraction and repulsion losses E_{ins} and E_{clo} .

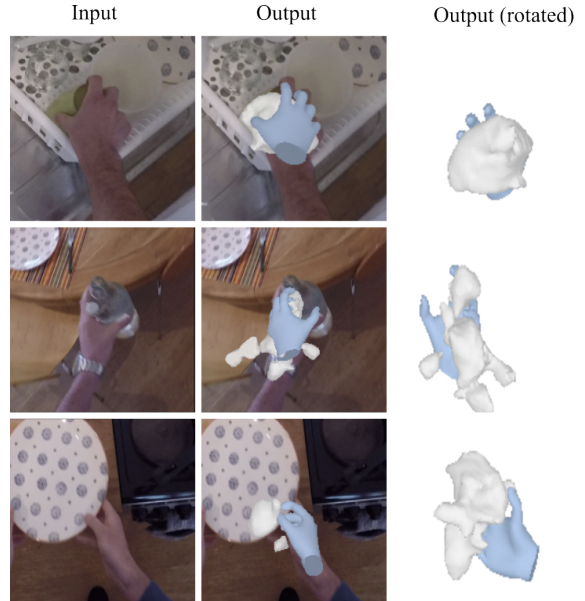


Figure 8. In-the-wild test of Ihoi [51]

The term E_{ins} ensures all object vertices are located inside the contact surface of the hand (Fig 9). For each $v_o \in V_o$, we locate the nearest vertex in hand contact regions, and compute distance along the surface normal of this hand vertex. Object vertices that penetrate into the contact surface will have negative values. We maximise those negative values, truncating the positive ones:

$$E_{ins}^n = \sum_{v_o \in V_o} -1 * \min(d_v, 0) \quad (13)$$

$$d_v = \langle v_o - v_h^*, n_h^* \rangle \quad (14)$$

where v_h^* is the corresponding nearest vertex on the hand and n_h^* is the surface normal of v_h^* .

In addition to E_{ins} , which pushes the object out of the penetrating region against the hand, we use a balancing loss E_{clo} which pulls the object to touch these contact regions. We here focus on the eight contact regions showcased in Fig 9. For each contact region with hand vertices $\{v_h\}_C$, the region-to-object distance is defined as the minimum distance of all (v_h, v_o) pairs. We use 5 finger tip regions and minimise the average of these region-to-object distances.

$$E_{clo}^n = \frac{1}{5} \sum_C d(\{v_h\}_C, V_o) \quad (15)$$

$$d(\{v_h\}_C, V_o) = \min_{v_h \in \{v_h\}_C, v_o \in V_o} \langle v_h - v_o, n_o \rangle \quad (16)$$

where n_o is the surface normal of v_o .



Figure 9. Eight contact regions: five finger tips + three palm areas. The contact regions serve two purposes: bounding the object inside and attracting the object closer to these regions.

Initialisation of poses on EPIC-Grasps For EPIC-Grasps dataset, we manually set initial object relative poses to the common poses of each category, results in 80 total initial poses for 9 object categories.